

# X-ray States of Black Hole Binaries in Outburst

R. A. Remillard

*MIT Kavli Institute for Astrophysics and Space Research*

**Abstract.** We continue to probe the properties of stellar-size black holes and the physics of black-hole accretion using bright X-ray transients. Progress has been made in the recognizing that the three states of active accretion are related to different physical elements that may contribute radiation: the accretion disk, a jet, and a compact corona. Each of these states offers potential applications for investigation via general relativity in the regime of strong gravity. High-frequency QPOs are especially interesting in this regard, as the evidence mounts for their interpretation as stationary ‘voice-prints’ that may constrain black-hole mass and spin.

**Keywords:** Physics of black holes, Black holes

**PACS:** 04.70.-s, 97.60.Lf

## RE-DEFINING X-RAY STATES

It has been proposed recently that X-ray states of black hole binary systems should be redefined in terms of quantitative criteria that utilize both X-ray energy spectra and power density spectra (PDS) [22]. The goals of this effort are to capture the essential elements of historical state descriptions, to incorporate the complexity of black hole behavior revealed in extensive monitoring campaigns with the *Rossi* X-ray Timing Explorer (*RXTE*), and to correct misleading terminology.

The redefinition of X-ray states utilizes four criteria:  $f_{disk}$ , the ratio of the disk flux to the total flux (both unabsorbed) at 2-20 keV; the power-law photon index ( $\Gamma$ ) at energies below any break or cutoff; the integrated rms power in the PDS at 0.1–10 Hz ( $r$ ; expressed as a fraction of the average source count rate); and the integrated rms amplitude ( $a$ ) of a QPO detected in the range of 0.1–30 Hz.

It had been known for decades that the energy spectra of outbursting black holes often exhibit composite spectra consisting of two broadband components [43]. There is a multi-temperature accretion disk [36, 19, 10] with a characteristic temperature near 1 keV. This modified form of the black-body function is easy to recognize. Usually, it is seen in combination with a quasi-power-law component, which may be modified by disk reflection [5, 33] and/or a cutoff energy (e.g. 100 keV) or a spectral break to a steeper power law. Many black hole systems further exhibit a broad Fe emission line (e.g. [34, 25]) and atomic absorption edges that are primarily due to the cold ISM. In some cases there are also absorption features due to hot gas that is local to the binary system (e.g. [18]).

There is a need to draw attention to those times when black hole radiation is dominated by the heat from the inner accretion disk, while there are no obvious temporal features that signify unexpected oscillations or instabilities that complicate the picture. Toward this end, the thermal state (formerly the “high/soft” state) is defined by the following three conditions: (1) the disk contributes more than 75% of the total unabsorbed flux at

GRO J1655-40

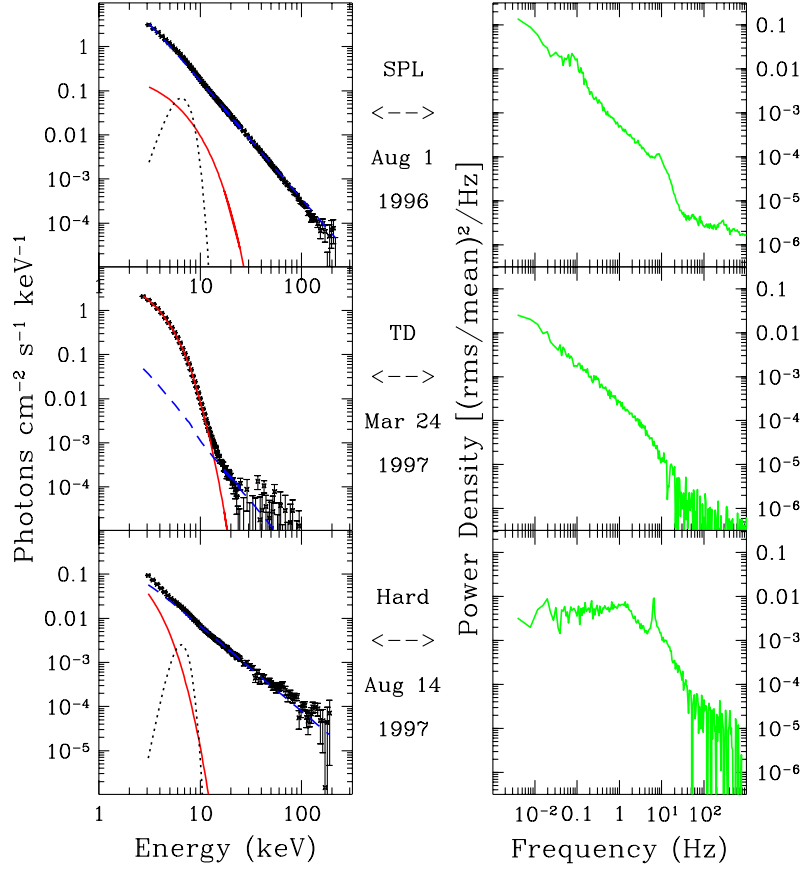


**FIGURE 1.** Examples of the 3 states of active accretion for the black hole binary GRO J1655-40. Left panels show the energy spectra, with model components attributed to thermal-disk emission (red solid line), a power-law continuum (blue dashes) and a relativistically broadened Fe K- $\alpha$  line (black dotted). Power-law components for the SPL and hard states are distinguished by different values of the photon index (i.e. slope). The PDS (green solid lines) are shown in the right panels. A strong, band-limited continuum characterizes the hard state, while QPOs and the absence of the intense, broad continuum are usually seen in the SPL state.

2–20 keV, i.e.  $f > 0.75$ , (2) there are no QPOs present with integrated amplitude above 0.5% of the mean count rate, i.e.  $a_{max} < 0.005$ , and (3) the integrated power continuum is low, with  $r < 0.06$ .

In principle, the normalization constant for the thermal component may allow numerical estimates of the radius of the inner accretion disk, if the source distance and disk inclination are accurately known [49]. However, such estimates depend on disk models computed under general relativity (GR), with careful attention to the inner disk boundary

condition and to effects of radiative transfer [23]. Improved disk models may one day lead to trustworthy results, and this could lead to measures of the dimensionless spin parameter when the mass is well constrained via dynamical measures of stellar motion in the binary system.

There are other occasions when the spectrum from an outbursting black-hole system shows a much greater contribution from an X-ray power-law component. Observations with *CGRO*–Ossie were particularly valuable in showing that there were two forms of these non-thermal spectra [12]. Spectral fits for the power-law component yield clusters of  $\Gamma$  values: one near 1.7 (hard state, with an exponential decrease beyond  $\sim 100$  keV) and the other near 2.5 (steep power law, with no apparent cutoff). In each case, the corresponding PDS also shows a distinct departure from the thermal state. An illustration of the thermal state and the two non-thermal states is given in Fig. 1.

In the hard X-ray state, the accretion-disk component is either absent or it is modified in the sense of appearing comparatively cool and large. The hard state has been clearly associated with the presence of a steady type of radio jet [7, 4]. Transitions to either the thermal state (e.g. GX339-4; [8, 3]) or an SPL state (e.g. Cyg X-1; [50]) effectively quenches the radio emission. This crucial, multi-frequency advancement helps to demonstrate that the three X-ray states of black hole binaries in outburst represent accretion systems that are very different in terms of physical elements, geometry, and energy-transport mechanisms. Hindsight analysis of X-ray data correlated with radio signatures of the steady jet allows a definition of the hard state, again based on three X-ray conditions: (1)  $f < 0.2$ , i.e. the power-law contributes at least 80% of the unabsorbed 2–20 keV flux, (2)  $1.5 < \Gamma < 2.1$  (for power-law, cutoff power law, or broken power-law (using  $\Gamma_1$ ), as appropriate), and (3) the PDS yields  $r > 0.1$ .

Current research on the hard state now addresses more detailed and physical questions such as the jet energetics and ejection velocities ([7]; see also Gallo et al., these proceedings), and the whether the X-ray spectrum represents synchrotron radiation, inverse Compton emission at the base of the jet, or a collimated outflow related to an advection-dominated accretion flow (ADAF) [6, 20, 9, 47].

The steep power law (SPL) component was first linked to the power-law “tail” found in the thermal state, and it was widely interpreted as inverse Compton radiation from a hot corona somehow coupled to the accretion disk. The picture became more complicated when X-ray QPOs were first detected with *Ginga* for two sources: GX339-4 (6 Hz) and X-ray Nova Muscae 1991 (3–8 Hz) [27, 26]. The QPOs, the high luminosity, and the strength of the power-law component prompted the interpretation that the QPOs signified a new black hole state, labeled as the “very high” state. *RXTE* observations later showed that X-ray QPOs from black-hole binaries are much more common than had been realized [45].

As noted above, *CGRO* observations have shown that the SPL may extend to photon energies as high as 800 keV [12, 44]). This forces consideration of non-thermal Comptonization models [11, 48]. The QPOs impose additional requirements for an oscillation mechanism that must be intimately tied to the electron acceleration mechanism (in the inverse Compton scenario), since the QPOs are fairly coherent ( $v/\Delta v \sim 12$ ; [32]) and are strongest above 6 keV. Despite a wide range in SPL luminosities, the SPL tend to dominate as the luminosity approaches the Eddington limit (e.g. Fig. 1). Furthermore, the occasions of high-frequency QPOs at 100-450 Hz in 7 black hole binaries almost

always coincide with a strong SPL spectrum [22]. Overall, the many fundamental differences between the thermal and SPL properties (see Fig. 1) force us to reject alternative state descriptions that unify thermal and SPL observations under a single “soft” state.

The results from intense monitoring campaigns for black-hole transients with *RXTE* motivated the redefinition of the very high state as the “SPL state” [22], with conditions: (1)  $\Gamma > 2.4$ , (2)  $r < 0.15$ , and (3) either  $f < 0.8$  while a QPO (0.1 to 30 Hz) is present in the PDS (with  $a > 0.01$ ), **or**  $f < 0.5$  with no QPOs (i.e. the disk contributes less than half of the flux). Generally, the accretion disk remains visible in the X-ray spectrum in the SPL state. There may be modifications to the thermal parameters ( $T_{in}, R_{in}$ ) during SPL episodes at high luminosity. In such cases, the disk appears unusually small and hot, and this is a likely artifact of radiative transfer effects that occur when the disk is viewed through a compact corona with moderate optical depth [17].

This quantitative framework for the three states of active accretion in black-hole binary systems is intended to tie X-ray states to each of the three broad-band spectral components that have a distinct physical origin and/or radiation mechanism. These states appear to demonstrate a capacity for quasi-stability, but observations exhibit their inherently transient nature. Clearly, the parameter ranges chosen for the three X-ray states leave substantial room for intermediate conditions. Conversely, we abandon the effort to pigeon-hole every observation into a well-defined state ; this perspective merely honors the complexity of black hole outbursts as seen in the *RXTE* era.

## TEMPORAL EVOLUTION OF X-RAY STATES

The temporal evolution of X-ray states for the case of GRO J1655-40 (1996-1997 outburst) is shown in Fig. 2. The ASM light curve is displayed in the top panel, while the unabsorbed flux derived from spectral fits to *RXTE* pointed observations are shown in the bottom panel. Here, the X-ray state is also represented via the choice of plotting symbol: thermal (red x), hard (blue square), steep power-law (green triangle), and any intermediate type (yellow circle). In this particular case, the two intermediate cases exhibit properties that lie between the thermal and SPL definitions.

The state assignments utilize spectral parameters obtained via the modeling prescriptions of Sobczak et al. 1999 [38]. There are a few differences here: all *RXTE* observations are considered (adding programs 10261 and 20187), newer versions of PCA response models are used, the analyses are restricted to PCU #2, and a model with broken power-law (rather than a simple power-law) is used for the beginning of the outburst, up to and including 1996 June 20. The observations are grouped into 67 data intervals, combining short observations that occur on the same day. However, the last three *RXTE* pointings (beginning 1997 Aug 29) are then excluded, since the source flux is below 2 mCrab and the uncertainties in the spectral parameters is large. These are very likely to be additional samples of the hard state. The statistics of the 64 state assignments shown in Fig. 2 are listed in Table 1.

The temporal evolution of X-ray states for XTE J1550-564 (1998-1999 outburst) is shown in Fig. 3, with content and state representations analogous to Fig. 2. For this source spectral modeling efforts follow Sobczak et al. 2000 [39]. The re-analysis again targets PCU #2, a broken power-law model is used when it improves the fit significantly,

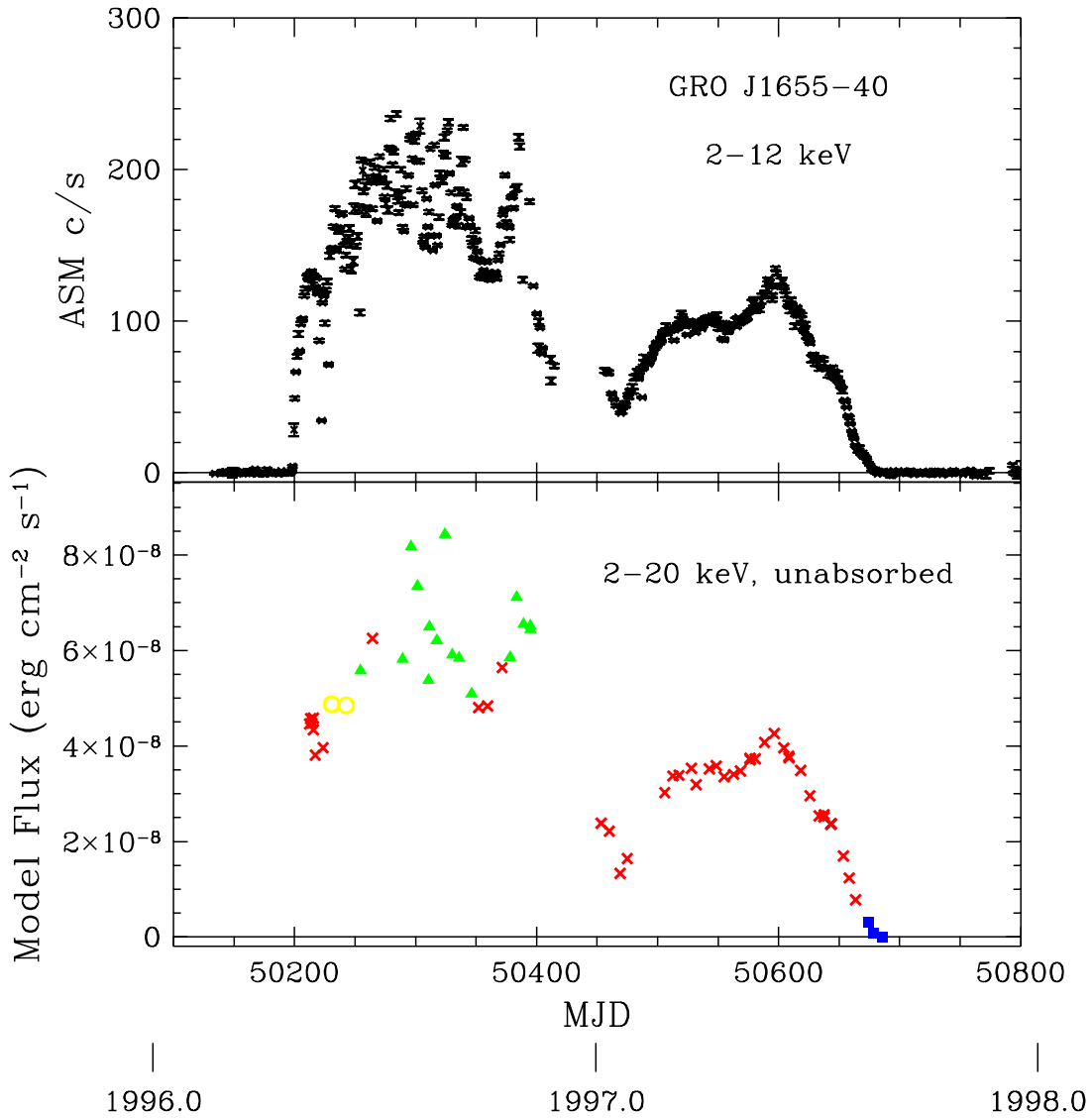


**FIGURE 2.** X-ray state evolution during the 1996-1997 outburst of GRO J1655-40. The top panel shows the ASM light curve. The bottom panel shows the model flux (2–20 keV, unabsorbed) from PCA pointed observations. Here the symbol type denoted the X-ray state: thermal (red x), hard (blue square), steep power-law (green triangle), and any type of intermediate state (yellow circle).

and this happens frequently for observations before MJD 51140. Some observations on the same day are grouped together, with a net of 201 data intervals, and the statistics of state assignments are included in Table 1. There are a relatively large number of intermediate states encountered during this outburst of XTE J1550-564, especially in the MJD range 51050–51140. The latter cases exhibit properties that lie between the

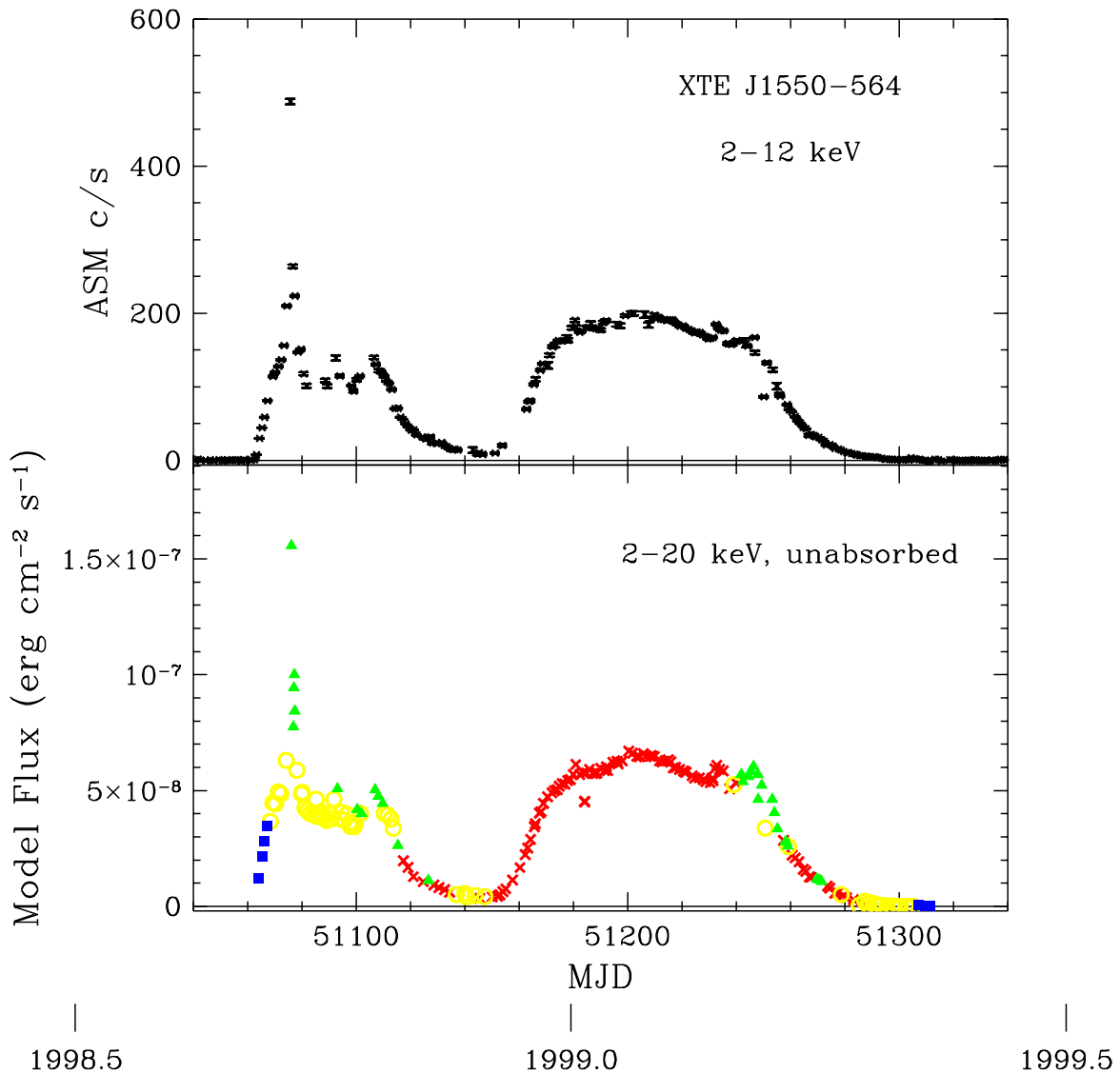


**FIGURE 3.** X-ray state evolution during the 1998-1999 outburst of XTE J1550-564. The top panel shows the ASM light curve. The bottom panel shows the model flux from PCA pointed observations, again with the X-ray state denoted as: thermal (red x), hard (blue square), steep power-law (green triangle), intermediate (yellow circle).

SPL and hard states (see [22] for more detailed discussions) and they coincide with the appearance of “C” type QPOs [32].

The 1998-1999 outburst of XTE J1550-564 was followed by successively weaker outbursts in 2000, 2001, 2002, and 2003. The outburst of 2000 again shows multi-state spectral evolution, but the three weaker outbursts appear entirely constrained to the hard

**TABLE 1.** Statistics of X-ray State Classifications

	Data intervals	Thermal state	SPL state	Hard state	Intermediate states
GRO J1655-40 (1996-1997)	64	43	16	3	2
XTE J1550-564 (1998-1999)	201	102	30	7	62

state (e.g. [2]).

## HIGH FREQUENCY QPOS FROM BLACK HOLE BINARIES

High-frequency QPOs (HFQPOs; 40-450 Hz) have been detected thus far in 7 black-hole binaries or candidates. These are transient subtle oscillations, with  $a \sim 1\%$  [28, 29, 13, 41, 42, 31, 14, 15, 30]. Frequently, one must select photon energy bands above 6 keV or above 13 keV in order to gain significant detection. Furthermore, for statistical reasons most detections require efforts to group observations with similar spectral and/or timing characteristics. All of the current detections for black-hole binaries are all displayed in Fig. 4. HFQPOs above 100 Hz generally occur during the SPL state [22].

Four sources (GRO J1655-40, XTE J1550-564, GRS 1915+105, and H1743-322) exhibit pairs of QPOs that have commensurate frequencies in a 3:2 ratio. These HFQPOs have frequencies above 100 Hz, and they generally occur during the SPL state [22]. GRS 1915+105 shows an additional, slower QPO pair (41 and 67 Hz) [28, 42] that occurs in thermal states with moderate to high luminosity,

In many cases, there is a substantial range in X-ray luminosity within a set of observations that contribute to a particular HFQPO, or a particular pair of commensurate HFQPOs in a given source (e.g. [31]). This supports the conclusion that HFQPO frequency systems are a stable timing signatures inherent to the accreting black hole. This is an important difference from the the kHz QPOs in neutron-star systems, which exhibit large variations in frequency. Moreover, the frequency stability of such a fast oscillations seems to suggest that HFQPOs may represent an invaluable means to probe black hole mass and spin via GR theory.

Commensurate HFQPO frequencies can be seen as a signature of an oscillation driven by some type of resonance condition. In fact, it has been proposed by Abramowicz & Kluzniak [1] that QPOs could represent a resonance in the coordinate frequencies given by GR for motions around a black hole under strong gravity (see [24]). Earlier work had used GR coordinate frequencies and associated beat frequencies to explain QPOs with variable frequencies in both neutron-star and black-hole systems [40].

The “parametric resonance” concept hypothesizes enhanced emissivity from accreting matter at a radius where two of the three coordinate frequencies (i.e. azimuthal, radial, and polar) have commensurate values that match (either directly or via beat frequencies) the observed QPOs. For the cases with known black hole mass, the value of the dimensionless spin parameter ( $a_*$ ) can be determined via the application of this resonance model if the correct pair of coordinate frequencies can be identified. In fact, reasonable values ( $0.25 < a_* < 0.95$ ) can be derived from the observed HFQPOs for either 2:1 or

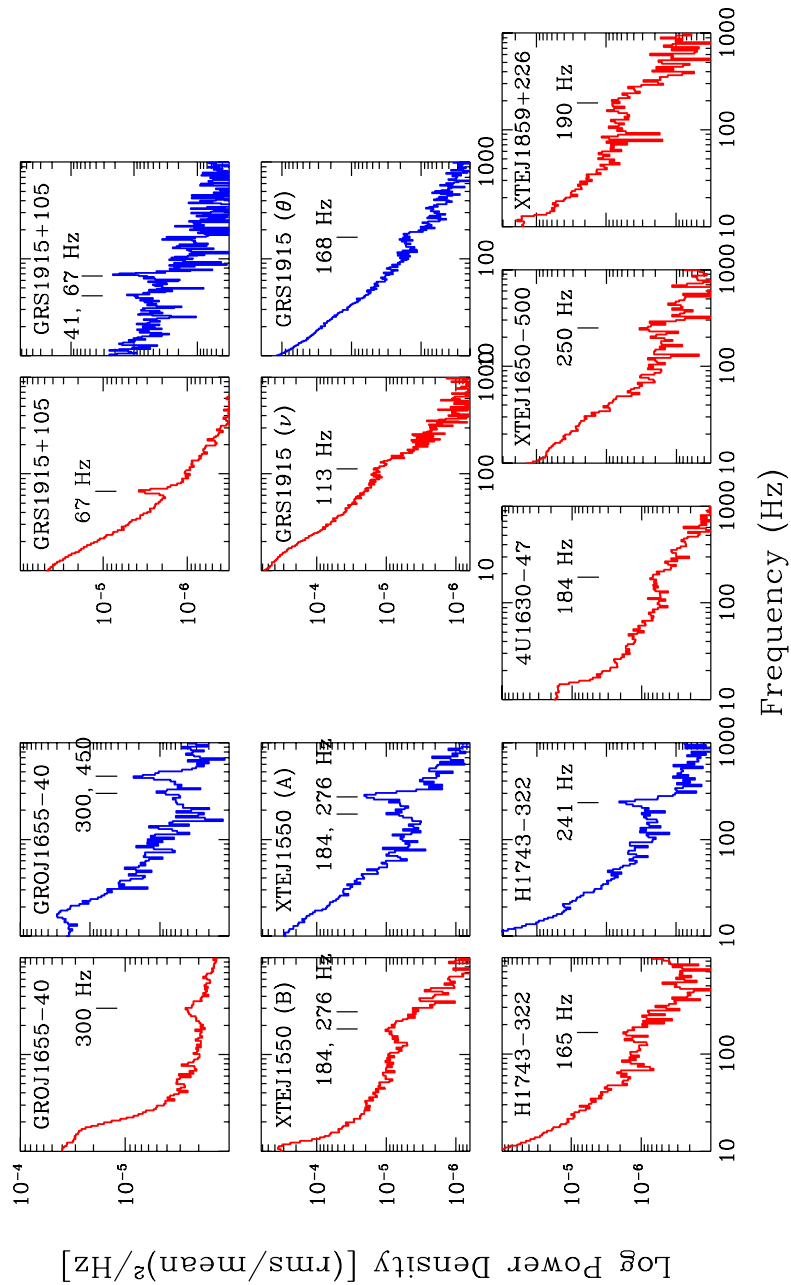


**FIGURE 4.** High frequency QPOs (40-450 Hz) seen in 7 black hole binary systems. PDS plotted in red are derived from the energy range 2–30 keV, while those in blue correspond with 13-30 keV, except for H1743-322 (6-30 keV). Four sources show pairs of HFQPOs with central frequencies that occur in a 3:2 ratio. GRS 1915+105 shows an additional pair at 41 and 67 Hz. It should be noted that we generally detect one QPO at a time, and QPOs involved in the 3:2 ratio tend to occur alternately, rather than simultaneously.



3:1 ratios in either orbital:radial or polar:radial coordinate frequencies [31].

The driving mechanism that would allow accretion blobs to grow and survive at the resonance radius has not been specified, and it is known that there are severe damping forces in the inner accretion disk [21]. On the other hand, ray-tracing calculations under GR [37] show that the putative blobs could indeed produce the HFQPO patterns, and that the choice of  $3 \times \nu_0$  versus  $2 \times \nu_0$  for the stronger QPO is governed by the angular width of the accreting blob. Clearly, there more work is needed to investigate this resonance model.

A possible alternative scenario is to extend the models for “diskoseismic” oscillations to include non-linear effects that might drive some type of resonant oscillation. Diskoseismology treats the inner disk as a resonance cavity in the Kerr metric ([16, 46]). Normal modes have been derived for linear perturbations, and the extension of this theory would be both very interesting and difficult. Another alternative is to consider accretion models that deviate from a thin disk geometry, e.g. an accretion torus and its oscillation modes under GR [35].

For three systems that show HFQPO pairs with frequencies in 3:2 ratio, we have the fortune of black hole mass estimates. In most types of GR oscillations, including the coordinate frequencies discussed above, the oscillation frequency scales with black-hole mass as  $M^{-1}$ , with additional dependence on the dimensionless spin parameter and the possibly the radius where the oscillations originate. Surprisingly, these three cases yield a relationship between HFQPO frequency and black hole mass that is consistent with a simple  $M^{-1}$  relationship [22]:  $\nu_0 = 931M^{-1}$ , where HFQPOs are seen at frequencies of  $2 \times \nu_0$  and  $3 \times \nu_0$ . This result suggests that these black holes have similar values of the dimensionless spin parameter. Furthermore, these results offer strong encouragement for efforts to interpret black-hole HFQPOs via GR theory.

## ACKNOWLEDGMENTS

This work was supported by the NASA contract to MIT for the ASM and EDS instruments on *RXTE*. Special thanks are extended to Jeff McClintock and Jeroen Homan for many helpful discussions.

## REFERENCES

1. M. A. Abramowicz, and W. Kluzniak, *A&A*, **374**, L19–L20 (2001).
2. T. Belloni, A. P. Colombo, J. Homan, S. Campana, and M. van der Klis, *A&A*, **390**, 199–204 (2002).
3. S. Corbel, et al., *A&A*, **359**, 251–268 (2000).
4. V. Dhawan, I. F. Mirabel, and L. F. Rodriguez, *Ap. J.*, **543**, 373–385 (2000).
5. C. Done, and S. Nayakshin, *MNRAS*, **328**, 616–622 (2001).
6. A. A. Esin, et al., *Ap. J.*, **555**, 483–488 (2001).
7. R. Fender, “Jets from X-ray binaries”, in *Compact Stellar X-ray Sources*, edited by W. H. G. Lewin and M. van der Klis, Cambridge University Press, Cambridge, 2005, in press (astro-ph/0303339).
8. R. Fender, et al., *Ap. J.*, **519**, L165–L168 (1999).
9. F. Frontera, et al., *Ap. J.*, **592**, 1110–1118 (2003).
10. M. Gierlinski, and C. Done, *MNRAS*, **347**, 885–894 (2004).
11. M. Gierlinski, and C. Done, *MNRAS*, **342**, 1083–1092 (2003).

12. J. E. Grove, W. N. Johnson, R. A. Kroeger, K. McNaron-Brown, and J. Skibo, *Ap. J.*, **500**, 899–908 (1998).
13. J. Homan, et al., *Ap. J. Suppl.*, **132**, 377–402 (2001).
14. J. Homan, et al., *Ap. J.*, **586**, 1262–1267 (2003).
15. J. Homan, et al., *Ap. J.*, in press (2005); (astro-ph/0406334).
16. S. Kato, *PASJ*, **53**, 1–24 (2001).
17. A. Kubota, and K. Makishima, *Ap. J.*, **601**, 428–438 (2004).
18. J. C. Lee, C. S. Reynolds, R. A. Remillard, N. S. Schulz, E. G. Blackman, and A. C. Fabian, *Ap. J.*, **567**, 1102–1111 (2002).
19. K. Makishima, et al., *Ap. J.*, **308**, 635–643 (1986).
20. S. Markoff, H. Falcke, and R. Fender, *A&A*, **372**, L25–L28 (2001).
21. D. Markovic, and F. K. Lamb, F.K., *Ap. J.*, **507**, 316–326 (1998).
22. J. E. McClintock, and R. A. Remillard, “Black Hole Binaries”, in *Compact Stellar X-ray Sources*, edited by W. H. G. Lewin and M. van der Klis, Cambridge University Press, Cambridge, 2005, in press (astro-ph/0306213).
23. A. Merloni, A. C. Fabian, and R. R. Ross, *MNRAS*, **313**, 193–197 (2000).
24. A. Merloni, M. Vietri, L. Stella, and D. Bini, *MNRAS*, **304**, 155–159 (2001).
25. J. M. Miller, et al., *Ap. J.*, **577**, L15–L18 (2002).
26. S. Miyamoto, S. Iga, S. Kitamoto, and Y. Kamado, *Ap. J.*, **403**, L39–L42 1993.
27. S. Miyamoto, and S. Kitamoto, *Ap. J.*, **374**, 741–743 1991.
28. E. H. Morgan, R. A. Remillard, and J. Greiner, *Ap. J.*, **482**, 993–1010 (1997).
29. R. A. Remillard, E. H. Morgan, J. E. McClintock, C. D. Bailyn, and J. A. Orosz, *Ap. J.*, **522**, 397–412 (1999).
30. R. A. Remillard, J. E. McClintock, J. A. Orosz, and A. M. Levine, *Ap. J.*, submitted; (astro-ph/0407025).
31. R. A. Remillard, M. P. Muno, J. E. McClintock, and J. A. Orosz, *Ap. J.*, **580**, 1030–1042 (2002).
32. R. A. Remillard, G. J. Sobczak, M. P. Muno, and J. E. McClintock, *Ap. J.*, **564**, 962–973 (2002).
33. M. Revnivtsev, M. Gilfanov, and E. Churazov, *A&A*, **380**, 520–525 (2001).
34. C. S. Reynolds, and M. A. Nowak, *Phys.Rept.*, **377**, 389–466 (2003).
35. L. Rezzolla, S’i Yoshida, T. J. Maccarone, and O. Zanotti, *MNRAS*, **344**, L37–L41 (2003).
36. N. I. Shakura, and R. A. Sunyaev, *A&A*, **24**, 337–366 (1973).
37. J. D. Schnittman, and E. Bertschinger, *Ap. J.*, **606**, 1098–1111 (2004).
38. G. J. Sobczak, J. E. McClintock, R. A. Remillard, C. D. Bailyn, and J. A. Orosz, *Ap. J.*, **520**, 776–787 (1999).
39. G. J. Sobczak, et al., *Ap. J.*, **544**, 993–1015 (2000).
40. L. Stella, M. Vietri, and S. M. Morsink, *Ap. J.*, **524**, L63–L66 (1999).
41. T. E. Strohmayer, *Ap. J.*, **552**, L49–L53 (2001).
42. T. E. Strohmayer, *Ap. J.*, **554**, L169–L172 (2001).
43. Y. Tanaka, and W. H. G. Lewin, “Black-hole Binaries”, in *X-ray Binaries*, edited by W. H. G. Lewin, J. van Paradijs, and E. P. J. van den Heuvel, Cambridge U. Press, Cambridge, 1995, pp. 126–174.
44. J. A. Tomsick, P. Kaaret, R. A. Kroeger, and R. A. Remillard, *Ap. J.*, **512**, 892–900 (1999).
45. M. van der Klis, “A Review of Rapid Variability in X-ray Binaries”, , in *Compact Stellar X-ray Sources*, edited by W. H. G. Lewin and M. van der Klis, Cambridge University Press, Cambridge, 2005, in press (astro-ph/0410551).
46. R. V. Wagoner, *Phys. Rept.*, **311**, 259–269 (1999).
47. F. Yuan, W. Cui, and R. Narayan, *Ap. J.*, in press (2005); (astro-ph/0407612).
48. A. A. Zdziarski, and M. Gierlinski, *PThPS*, **155**, 99–119 (2004).
49. S. N. Zhang, W. Cui, and W. Chen, *Ap. J.*, **482**, L155–L158 (1997).
50. S. N. Zhang, et al., *Ap. J.*, **477**, L95–L98 (1997).